Editors' Suggestion | Featured in Physics

Robustness and Universality in Organelle Size Control

Kiandokht Panjtan Amiri, Asa Kalish, and Shankar Mukherji*
Department of Physics, Washington University in St. Louis, St. Louis, Missouri 63130, USA and Department of Cell Biology & Physiology, Washington University School of Medicine, St. Louis, Missouri 63110, USA

(Received 11 November 2021; accepted 7 November 2022; published 6 January 2023)

One of the grand challenges in cellular biophysics is understanding the precision with which cells assemble and maintain subcellular structures. Organelle sizes, for example, must be flexible enough to allow cells to grow or shrink them as environments demand yet be maintained within homeostatic limits. Despite identification of molecular factors that regulate organelle sizes we lack insight into the quantitative principles underlying organelle size control. Here we show experimentally that cells can robustly control average fluctuations in organelle size. By demonstrating that organelle sizes obey a universal scaling relationship we predict theoretically, our framework suggests that organelles grow in random bursts from a limiting pool of building blocks. Burstlike growth provides a general biophysical mechanism by which cells can maintain on average reliable yet plastic organelle sizes.

DOI: 10.1103/PhysRevLett.130.018401

Among the most critical scales of biological organization in the eukaryotic cell is its compartmentalization into organelles. Organelle biogenesis, among the most complex tasks the eukaryotic cell performs, is the result of the coordinated synthesis of tens to hundreds of protein and lipid macromolecular species, each of which is potentially subject to stochastic fluctuations intrinsic to their production. Generally speaking, how these molecular-scale fluctuations propagate to micron-scale cellular geometric properties remains an outstanding question in quantitative cell biology and biophysics [1–4]. We have previously shown that organelle copy number statistics exhibit substantial cell-to-cell variability [5], though the root mechanisms of this variability remain the subject of much debate [6,7]. Here we turn our attention to the ability of the eukaryotic cell to control a closely linked biophysical property that determines organelle function: organelle size.

Pioneering work on a wide variety of organelles has focused on characterizing average organelle sizes and has begun to unravel the molecular mechanisms underpinning this size control [8]. The importance of controlling organelle size is further suggested by the many scaling relationships that have shown both fixed relative sizes of various organelles compared to their host cells in a variety of organisms and developmental contexts [9], including for the nucleus [10,11] and vacuole [12], and nontrivial relationships such as maximal mitochondrial activity in intermediate sized cells [13]. Uncoordinated regulation of organelle size can lead to severe phenotypic defects, such as impaired *Chlamydomonas reinhardtii* motility in uncoordinated flagellar length control [14], inappropriately sized secretory vesicles due to variability in Golgi size [15], and impaired metabolism due to defects in mitochondrial [16] and peroxisomal fission [17] among others. What remains underexplored is development of a quantitative understanding of the precision with which organelle size variability is controlled, particularly for organelles that exist in multiple copies per cell.

Drawing on a combination of the theory of stochastic processes and quantitative fluorescence imaging, we directly examine two questions: how precisely does the cell control the sizes of its organelles and what, if any, overarching quantitative principles collectively describe the patterns of observed organelle sizes despite the vastly different molecular mechanisms that implement size control?

In order to decipher the quantitative principles governing organelle size control, we reasoned that we could use a mathematical model of organelle biogenesis to interpret endogenous stochastic fluctuations in organelle size. Our first task in building a mathematical framework to quantify organelle size control was to be able to distinguish between the three general limits organelle growth is thought to fall into [8]. In the first limit, termed constant growth, organelle growth occurs at a constant rate. In the second limit, termed negative feedback control, the cell constrains organelle growth rates to drive them toward a target size. In the third limit, termed the limiting pool, we assume that organelle sizes are constrained by a limiting pool of building blocks from which they are assembled. In each limit, organelle size is affected by both size-specific processes, such as growth and disassembly, as well as number changing processes such as fission and fusion [18,19]. We therefore derived a stochastic model of organelle biogenesis that tracks the joint probability distribution of organelle numbers and sizes in single simulated cells. In this model organelles can be created *de novo*, decay, undergo fission and fusion, grow in size, and shrink. Using the Gillespie algorithm [20] we solve our model for the three general limits that organelle

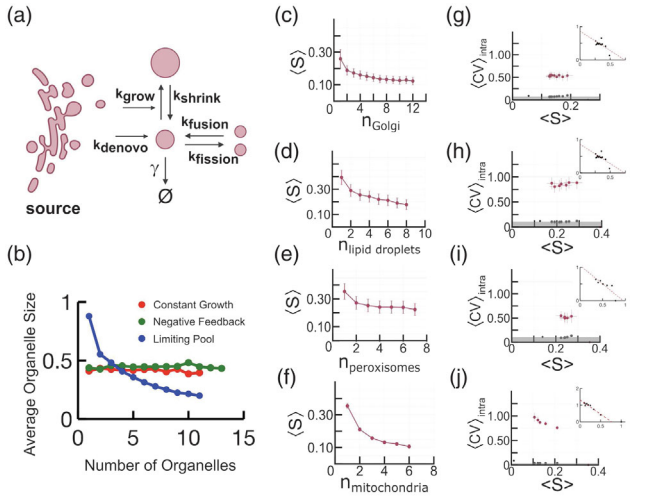

FIG. 1. (a) Schematic of biophysical processes in model of organelle biogenesis. (b) Gillespie simulation results of organelle size versus number for 3 classes of organelle size models. (c)–(f) Average organelle size versus organelle number. (g)–(j) Average intracellular CV versus organelle size. Organelle sizes are normalized to largest organelle size of a given type. Gray data points indicate errors in CV propagated from estimated errors in organelle size and gray region is the average value of the gray CV error data points. Star indicates measured CV of diffraction limited 100 nm beads.

growth can take. The simulation is performed by tracking the number and sizes of organelles in a single cell until they reach steady state.

Inspired by physiologically relevant cases, we focused the simulations on three different regimes of number changing dynamics: in the late Golgi [21,22] and lipid droplet [23–25] relevant case in which number dynamics are governed by *de novo* synthesis and first order decay [Fig. 1(a)]; in the peroxisome relevant limit of when organelle numbers change through *de novo* synthesis, first order decay, and fission (see Refs. [26–29] and Fig. S1A in Supplemental Material [30]); and lastly in the mitochondria relevant limit of when the abundance of organelles changes solely through fission and fusion (see Refs. [31–33] and Fig. S1B [30]). For each number changing regime we see that the correlation between fluctuations in organelle number and average organelle size is diagnostic for whether organelles grow at a constant rate or are constrained by either negative feedback or a limiting pool of building blocks. Most importantly, in the limiting pool limit we observe a negative correlation between organelle number and average organelle size [Fig. 1(b)]. This contrasts with the constant growth and negative feedback regimes, in which average organelle size is constant in simulated cells with different organelle numbers when organelles are made *de novo* [Fig. 1(b)]. The model thus leaves us well positioned to use experimental data to infer which growth limit describes a given organelle.

To experimentally measure joint organelle number versus size distributions so as to infer organelle growth rules with our model, we analyzed the endogenous stochastic fluctuations in organelle numbers and sizes in the budding yeast *Saccharomyces cerevisiae*. To visualize the various organelles we examine, we fuse the fluorescent protein monomeric Kusibara Orange2 (mKO2) to organelle membrane resident proteins (Fig. S2 [30]). We use a Bayesian image analysis framework [34] (Fig. S3 [30]) to analyze the micrographs and obtain joint single cell average organelle size versus organelle number probability distributions of fluorescently labeled late Golgi (labeled with Sec7-mKO2; Fig. S4 [30]), lipid droplets (Erg6-mKO2; Fig. S5 [30]), peroxisomes (Pex3-mKO2; Fig. S6 [30]), and mitochondria (Tom70-mKO2; Fig. S7 [30]). From these joint distributions we plot the average organelle size as a function of organelle number. For each of the organelles we examine, we observe a significant negative correlation between organelle number and average organelle size [Figs. 1(c)–1(f)]. This negative correlation between number and size persists for peroxisomes even when peroxisome fission is inhibited (Figs. S8A-S8C [30]). Our measurements suggest that the sizes of the four organelles under study are all constrained by a limiting pool of building blocks.

Among the most attractive hypotheses arguing for the utility of the limiting pool model of organelle growth is that it achieves a stable organelle size in the absence of feedback. However, it has been shown theoretically that growing multiple organelles from a limiting pool of building blocks can lead to remarkably severe size fluctuations between organelles within the same cell [35,36], potentially impairing cellular-scale physiological function. To quantify how intracellular fluctuations in organelle size behave in our model, we plot the average intracellular coefficient of variation (CV) in organelle size as a function of organelle size in cells with equal numbers of organelles [Figs. 1(g)–1(j), insets]. We focus on cells simulated in the limiting pool limit of the model. As expected for a Poisson-type process, we observe that for decreasing organelle size (which corresponds to increasing organelle number) the intracellular organelle size CV increases. This suggests that cells face a fundamental trade-off in their ability to achieve organelle size homeostasis.

We then use our experimental joint distributions of organelle number and size for the late Golgi, lipid droplets, mitochondria, and peroxisomes to directly measure the CV of organelle sizes within single cells [Figs. 1(g)–1(j) herein and Figs. S9 and S10 in Ref. [30]]. Contrary to our theoretical expectation [Figs. 1(g)–1(j), insets], we see that the average intracellular CV of the late Golgi, lipid droplets, and peroxisomes remain constant with varying average organelle size. We reproduced these average intracellular CV profiles using multiple imaging modalities, including superresolution radial fluctuation imaging (see Ref. [37]

and Fig. S9 [30]), and with multiple organelle markers, including alternative fluorescently labeled organelle-resident proteins and dyes that localize to specific organelle membranes (Fig. S10 [30]). Thus we conclude that, despite organelles changing in size by twofold, cells are able to robustly maintain proportionality in the fluctuations in sizes to within a factor of 0.5 (peroxisomes) to 0.6 (late Golgi and lipid droplets) of the mean organelle size, thereby avoiding a rise in intracellular fluctuations when the mean organelle size shrinks. Only the average intracellular CV of mitochondria appears to increase when the cell creates more, smaller copies of this organelle.

To address the discrepancy between the noise profile resulting from our model versus the noise profile of organelles observed experimentally, we consider a fundamental revision to how organelle growth proceeds in our mathematical framework. Following ruling out a wide variety of alternative growth models with deterministic growth steps (Fig. S11 [30]), we sought models that would allow for independent regulation of growth timing and growth magnitudes that would allow fluctuations to not depend strictly on mean organelle size. Building on previous observations that subcellular structures can grow from bursts of random sizes of building blocks [38], we constructed a model in which organelles grow from a limiting pool of building blocks in exponentially distributed bursts of random size characterized by an average size β that occur at random times characterized by a burst frequency α [Fig. 2(a)], similar to previous models of transcriptional bursting [39]. In the model, to implement the limiting pool constraint we make the average burst size β proportional to the free pool of building blocks available for organelle growth.

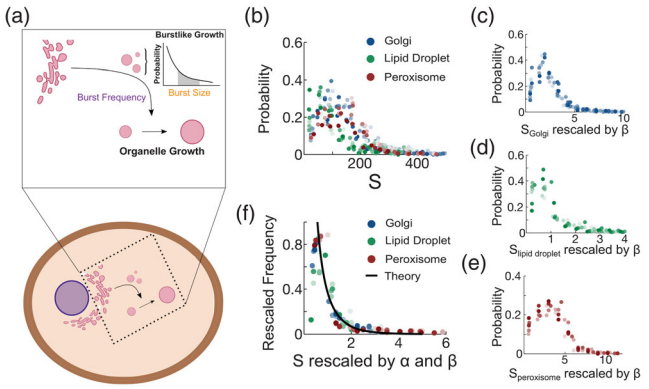

FIG. 2. (a) Schematic of burstlike model of organelle growth. (b) Distributions of experimentally measured late Golgi, lipid droplet, and peroxisome sizes. Size of 500 voxels corresponds to 0.4 μm^3. (c) Histograms of late Golgi, (d) lipid droplet, and (e) peroxisome sizes rescaled by their experimentally derived organelle-specific burst sizes. (f) Histogram of organelle size distributions rescaled by both experimentally derived organelle-specific burst sizes and burst frequencies; black curve is the theoretically predicted scaling relationship from the model.

We then proceeded to solve this model for the steady state organelle size distribution. If the limiting pool of building blocks is not exhausted and allows organelle sizes to fluctuate independently of each other, and if copy number changes are slow compared to size changes [40–45], then the resulting steady state organelle size distribution from cells that contain a defined number of organelles can be solved analytically and follows a γ distribution [30]. Each steady state γ distribution corresponding to a subpopulation of cells with defined organelle number has a mean size $\alpha\beta$ [Fig. 2(b) herein and Fig. S12 in Ref. [30]]. Crucially, however, one can show that for γ distributions the $\mathrm{CV} = 1/\sqrt{\alpha}$. This allows the cell to decouple the average fluctuations in intracellular organelle size from the mean organelle size as we observe experimentally in the cases of the Golgi apparatus, lipid droplets, and peroxisomes but not the mitochondria, allowing robust tuning of organelle sizes if they are modulated by changes in β but not α. Moreover, because we measure the CV, and thus α, and the mean organelle size, and thus $\alpha\beta$, both model parameters can be inferred solely through measurements without any model fitting required. We note that while the separation of timescales renders the model solvable analytically, the main results, in which organelle intracellular CVs are invariant to average organelle size and organelle sizes are γ distributed, allow for number changing processes (Fig. S12 [30]).

The model predicts that we should observe two types of data collapse upon rescaling organelle sizes (Figs. S13A–S13G [30]) in the cases of the Golgi apparatus, lipid droplets, and peroxisomes. First, since the model holds that organelle sizes change only through modulation of burst sizes, rescaling organelle sizes by their corresponding burst sizes should collapse them onto unifying γ distributions specific to each organelle. Second, by further rescaling these organelle-specific size distributions by their organelle-specific burst frequencies, our whole collection of late Golgi, lipid droplet, and peroxisome sizes should collapse onto the universal curve $f(\tilde{S}) = (e^{-\tilde{S}}/\tilde{S})$, where $\tilde{S}$ is the dimensionless rescaled organelle size [30].

To test our prediction that modulation of burst size alone can explain changes in organelle sizes, we first use our experimental data to obtain burst size values for each late Golgi, peroxisome, and lipid droplet size distribution. We then rescale late Golgi, peroxisome, and lipid droplet sizes by their experimentally inferred burst sizes and plot the resulting rescaled size distribution. We see that late Golgi, lipid droplet, and peroxisome sizes collapse onto single γ distributions [Figs. 2(c)–2(e)]. Further rescaling the organelle-specific rescaled size histograms by their experimentally calculated burst frequencies, we see that despite the starkly different molecular mechanisms by which their sizes are controlled, late Golgi, lipid droplet, and peroxisome size distributions further collapse onto the single theoretically predicted universal curve $f(\tilde{S}) = (e^{-\tilde{S}}/\tilde{S})$

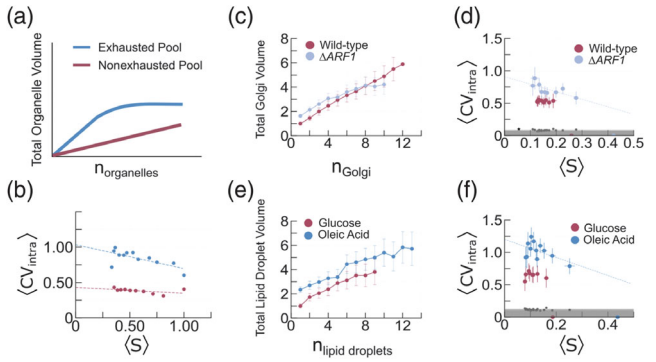

FIG. 3. (a) Total organelle size V as a function of the number of organelles in the limits where the pool is exhausted (blue line) versus nonexhausted (maroon line). (b) Average intracellular CV of organelle sizes versus average organelle sizes in 500 simulated cells from the burstlike model, when pool is exhausted versus nonexhausted. Total organelle size (c) and (d) average intracellular size CV of late Golgi from populations of wild-type (maroon) and $\Delta ARF1$ (purple) cells. (e) Total organelle size and (f) average intracellular size CV of lipid droplets marked with Erg6-mRFP from populations of wild-type cells grown in glucose (maroon) and in medium with 0.2 percent oleic acid (blue).

[Fig. 2(f)]. This fitting parameter-free data collapse strongly suggests that our mathematical model of organelle biogenesis has captured an essential, unifying feature of endomembrane organelle growth regulation.

According to our model, sufficient capacity in the limiting pool of building blocks allows organelles to grow and fluctuate in size independently of each other and allows for robust intracellular size control [Fig. 2(a)]. Our model also predicts, however, that if the available amount of building blocks for growth depletes enough [Fig. 3(a)] then intracellular organelle size fluctuations will become anticorrelated. Anticorrelated fluctuations, in turn, will lead to a rise in the average intracellular CV as shown in our simulation results [Fig. 3(b)].

To test our prediction that organelle growth from a limiting pool with little spare capacity leads to an elevated intracellular CV, we examine the case of mitochondria, whose sizes are a balance between biomass conserving fission and fusion. We plot total organelle volume versus organelle number for mitochondria and observe a line whose slope is much smaller than the slope of the line connecting the origin to the average organelle size when only 1 organelle is present (Fig. S14A [30]), consistent with the idea that cells largely rearrange existing fixed pool of mitochondrial biomass when changing mitochondrial number through fission and fusion. The resulting organelle size distributions are consistent with our model (Figs. S14D–S14N [30]) and with our observation of an increasing intracellular CV with decreasing mitochondria size [Fig. 1(j)].

Next, we test our prediction that depletion of the available supply of building blocks increased average intracellular Golgi CV. To test this idea, we analyze the late Golgi in cells lacking the vesicular traffic regulator $ARF1$ [40]. We reason that inhibiting retrograde intra-Golgi vesicular traffic mediated by the coat protein complex COPI through deleting $ARF1$ should result in an increased burst size at a reduced burst frequency [40,42,46]. At a given mean Golgi size, therefore, we expect that the reduced burst frequency will increase the CV. Deletion of $ARF1$ results in a statistically significant reduction in slope between total Golgi volume and Golgi number, especially at high Golgi number, indicating pool depletion [Fig. 3(c) herein and Fig. S15 in Ref. [30]]. We observe, in agreement with our hypothesis, that upon deletion of $ARF1$ the average intracellular Golgi size CV increases as the average Golgi size decreases [Figs. 3(c) and 3(d)].

Finally, to test our prediction that pool depletion leads to an elevated intracellular organelle size CV, we turn to lipid droplets. Lipid droplets are dynamic organelles whose sizes and copy numbers increase upon cellular exposure to long chain fatty acid-rich environments [24,25], and unlike peroxisomes are not thought to undergo fission events that would make our results difficult to interpret. We hypothesized that culturing cells in an oleic acid-rich environment could expose capacity constraints in lipid droplet biogenesis given our previous observation that these organelles appear to grow from a limiting pool of building blocks. To facilitate image analysis, we imaged lipid droplets with spinning disk confocal microscopy, using strains bearing lipid droplets fluorescently labeled with Erg6 fused to monomeric red fluorescent protein (Erg6-mRFP). We observe that when grown in glucose, lipid droplets do not expose capacity constraints in the limiting pool of building blocks. When grown in medium rich in oleic acid, total organelle volume increases and shows signatures of pool depletion [Fig. 3(e) herein and Fig. S15 in Ref. [30]], namely, a decrease in the rate of total organelle volume growth with respect to organelle number compared to cells grown in glucose. Concomitantly, we observe that the lipid droplet and peroxisome average intracellular organelle size CV increases with decreasing mean organelle size [Fig. 3(f)].

To establish the evolutionary conservation of our observed pattern of robustness in organelle size, we leveraged single cell imaging data from human induced pluripotent stem cells (iPSC) whose Golgi apparatus and mitochondria are labeled available from the Allen Cell Atlas [47]. With single cell organelle size distributions from populations of iPSCs, we are able to construct datasets of both average organelle size versus organelle number and the average intracellular organelle size CV as we have done for budding yeast. Both the Golgi apparatus and mitochondria yield negative sloping average organelle size versus organelle number curves consistent with a limiting pool model constraining their growth [Figs. 4(a) and 4(c)]. Most significantly, we observe that the average intracellular organelle size CV exhibits the

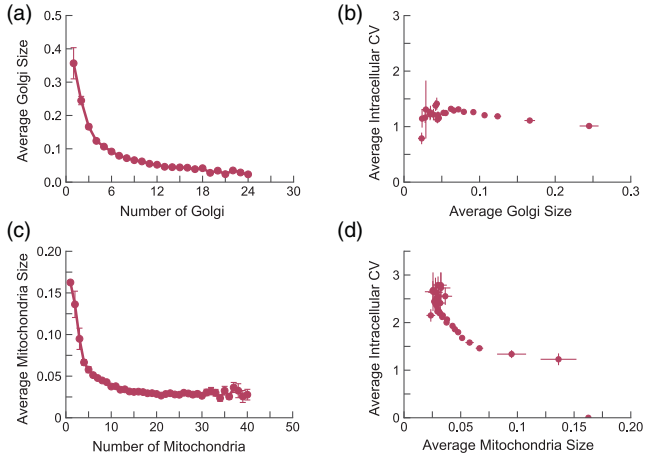

FIG. 4. (a) Average Golgi size versus number of Golgi from images of single induced pluripotent stem cells taken from the Allen Cell Atlas. (b) Average Golgi intracellular size CV versus average Golgi size. (c) Average mitochondrial size versus number of mitochondria from images of single induced pluripotent stem cells taken from the Allen Cell Atlas. (d) Average mitochondrial intracellular size CV versus average mitochondrial size.

same pattern in human iPSCs as seen for budding yeast: a robust, invariant organelle size CV as a function of average organelle size for the Golgi [Fig. 4(b)] and a sensitive, inverse correlation between organelle size CV and average organelle size for the mitochondria [Fig. 4(d)].

In order to explain our observed invariance of average organelle size fluctuations to changing mean organelle size, we propose a model in which organelle growth proceeds in a burstlike fashion from a limiting pool of building blocks. The pattern of organelle size robustness is shared between budding yeast and human iPS cells. The underlying molecular mechanisms producing these bursts are yet to be fully elucidated and are likely to be organelle specific and potentially species specific: Golgi size, for example, is likely influenced by both small increases in size from nonvesicular traffic as well as the sudden, large increases in size from vesicle fusion as we have shown here, while lipid droplet size bursts may result from burstlike expression of genes such as those encoding neutral lipid synthesis enzymes. However, the size statistics of a diverse array of organelles appear to be well described by a single unifying model that can be used to interpret future studies on the mechanistic underpinnings of organelle size control and a basis for more sophisticated modeling efforts to more accurately capture details suppressed here [6,7,48,49] as well as comparison to universal growth phenomena in seemingly unrelated biological systems [50]. More generally, burstlike synthesis and activity are ubiquitously observed in biophysical systems, from gene expression to the dynamics of neurons, and our observations here on the ability of burstlike processes to allow living systems to independently tune signal and noise may be leveraged much more broadly across diverse biological contexts.

We thank D. Laman Trip, T. Maire, and H. Youk for critically reviewing our Letter. This was was supported by NIH R35GM142704 (to S. M.). K. P. A. was supported by a fellowship from the Center for Science and Engineering of Living Systems at Washington University in St. Louis.

K. P. A. and A. K. contributed equally to this work.

*smukherji@physics.wustl.edu

[1] Amy Y. Chang and Wallace F. Marshall, Organelles—Understanding noise and heterogeneity in cell biology at an intermediate scale, J. Cell Sci. **130**, 819 (2017).
[2] Quentin Vagne and Pierre Sens, Stochastic model of maturation and vesicular exchange in cellular organelles, Biophys. J. **114**, 947 (2018).
[3] Himani Sachdeva, Mustansir Barma, and Madan Rao, Nonequilibrium description of de novo biogenesis and transport through Golgi-like cisternae, Sci. Rep. **6**, 38840 (2016).
[4] David Bauer, Hiroaki Ishikawa, Kimberly A. Wemmer, Nathan L. Hendel, Jane Kondev, and Wallace F. Marshall, Analysis of biological noise in the flagellar length control system, iScience **24**, 102354 (2021).
[5] Shankar Mukherji and Erin K. O'Shea, Mechanisms of organelle biogenesis govern stochastic fluctuations in organelle abundance, eLife **3**, e02678 (2014).
[6] Sandeep Choubey, Dipjyoti Das, and Saptarshi Majumdar, Cell-to-cell variability in organelle abundance reveals mechanisms of organelle biogenesis, Phys. Rev. E **100**, 022405 (2019).
[7] C. Jeremy Craven, Evaluation of predictions of the stochastic model of organelle production based on exact distributions, eLife **4**, e10167 (2015).
[8] Wallace F. Marshall, Cell geometry: How cells count and measure size, Annu. Rev. Biophys. **45**, 49 (2016).
[9] Daniel L. Levy and Rebecca Heald, Mechanisms of intracellular scaling, Annu. Rev. Cell Dev. Biol. **28**, 113 (2012).
[10] Daniel L. Levy and Rebecca Heald, Nuclear size is regulated by importin α and Ntf2 in *Xenopus*, Cell **143**, 288 (2010).
[11] Pan Chen, Miroslav Tomschik, Katherine M. Nelson, John Oakey, Jesse C. Gatlin, and Daniel L. Levy, Nucleoplasmin is a limiting component in the scaling of nuclear size with cytoplasmic volume, J. Cell Biol. **218**, 4063 (2019).
[12] Yee-Hung M. Chan, Lorena Reyes, Saba M. Sohail, Nancy K. Tran, and Wallace F. Marshall, Organelle size scaling of the budding yeast vacuole by relative growth and inheritance, Curr. Biol. **26**, 1221 (2016).
[13] Teemu P. Miettinen and Mikael Björklund, Cellular allometry of mitochondrial functionality establishes the optimal cell size, Dev. Cell **39**, 370 (2016).
[14] A. McVittie, Flagellum mutants of *Chlamydomonas reinhardtii*, J. Gen. Microbiol. **71**, 525 (1972).
[15] Francesco Ferraro, Janos Kriston-Vizi, Daniel J. Metcalf, Belen Martin-Martin, Jamie Freeman, Jemima J. Burden,

David Westmoreland, Clare E. Dyer, Alex E. Knight, Robin Ketteler, and Daniel F. Cutler, A two-tier Golgi-based control of organelle size underpins the functional plasticity of endothelial cells, Dev. Cell **29**, 292 (2014).

[16] Chitoku Toda, Jung Dae Kim, Daniela Impellizzeri, Salvatore Cuzzocrea, Zhong-Wu Liu, and Sabrina Diano, UCP2 regulates mitochondrial fission and ventromedial nucleus control of glucose responsiveness, Cell **164**, 872 (2016).

[17] Hans R. Waterham, Janet Koster, Carlo W. T. van Roermund, Petra A. W. Mooyer, Ronald J. A. Wanders, and James V. Leonard, A lethal defect of mitochondrial and peroxisomal fission, N. Engl. J. Med. **356**, 1736 (2007).

[18] Susanne M. Rafelski and Wallace F. Marshall, Building the cell: Design principles of cellular architecture, Nat. Rev. Mol. Cell Biol. **9**, 593 (2008).

[19] Martin Lowe and Francis A. Barr, Inheritance and biogenesis of organelles in the secretory pathway, Nat. Rev. Mol. Cell Biol. **8**, 429 (2007).

[20] Daniel Gillespie, Exact stochastic simulation of coupled chemical reactions, J. Chem. Phys. **81**, 2340 (1977).

[21] Brooke J. Bevis, Adam T. Hammond, Catherine A. Reinke, and Benjamin S. Glick, *De novo* formation of transitional ER sites and Golgi structures in *Pichia pastoris*, Nat. Cell Biol. **4**, 750 (2002).

[22] O. W. Rossanese, J. Soderholm, B. J. Bevis, I. B. Sears, J. O'Connor, E. K. Williamson, and B. S. Glick, Golgi structure correlates with transitional endoplasmic reticulum organization in *Pichia pastoris* and *Saccharomyces cerevisiae*, J. Cell Biol. **145**, 69 (1999).

[23] Albert Pol, Steven P. Gross, and Robert G. Parton, Review: Biogenesis of the multifunctional lipid droplet: Lipids, proteins, and sites, J. Cell Biol. **204**, 635 (2014).

[24] Florian Wilfling, Joel T. Haas, Tobias C. Walther, and Robert V. Farese, Jr., Lipid droplet biogenesis, Curr. Opin. Cell Biol. **29**, 39 (2014).

[25] Tobias C. Walther, Jeeyun Chung, and Robert V. Farese, Jr., Lipid droplet biogenesis, Annu. Rev. Cell Dev. Biol. **33**, 491 (2017).

[26] Dominic Hoepfner, Danny Schildknegt, Ineke Braakman, Peter Philippsen, and Henk F. Tabak, Contribution of the endoplasmic reticulum to peroxisome formation, Cell **122**, 85 (2005).

[27] Adabella van der Zand, Jürgen Gent, Ineke Braakman, and Henk F. Tabak, Biochemically distinct vesicles from the endoplasmic reticulum fuse to form peroxisomes, Cell **149**, 397 (2012).

[28] Alison M. Motley and Ewald H. Hettema, Yeast peroxisomes multiply by growth and division, J. Cell Biol. **178**, 399 (2007).

[29] Kasinath Kuravi, Shirisha Nagotu, Arjen M. Krikken, Klaas Sjollema, Markus Deckers, Ralf Erdmann, Marten Veenhuis, and Ida J. van der Klei, Dynamin-related proteins Vps1p and Dnm1p control peroxisome abundance in *Saccharomyces cerevisiae*, J. Cell Sci. **119**, 3994 (2006).

[30] See Supplemental Material at http://link.aps.org/supplemental/10.1103/PhysRevLett.130.018401 for details of experimental methods, data analysis, and mathematical model.

[31] Francisca Diaz and Carlos T. Moraes, Mitochondrial biogenesis and turnover, Cell Calcium **44**, 24 (2008).

[32] J. Nunnari, W. F. Marshall, A. Straight, A. Murray, J. W. Sedat, and P. Walter, Mitochondrial transmission during mating in *Saccharomyces cerevisiae* is determined by mitochondrial fusion and fission and the intramitochondrial segregation of mitochondrial DNA, Mol. Biol. Cell **8**, 1233 (1997).

[33] Susanne M. Rafelski, Matheus P. Viana, Yi Zhang, Yee-Hung M. Chan, Kurt S. Thorn, Phoebe Yam, Jennifer C. Fung, Hao Li, Luciano da F. Costa, and Wallace F. Marshall, Mitochondrial network size scaling in budding yeast, Science **338**, 822 (2012).

[34] M. P. Hobson and C. McLachlan, A Bayesian approach to discrete object detection in astronomical data sets, Mon. Not. R. Astron. Soc. **338**, 765 (2003).

[35] Lishibanya Mohapatra, Thibaut J. Lagny, David Harbage, Predrag R. Jelenkovic, and Jane Kondev, The limiting-pool mechanism fails to control the size of multiple organelles, Cell Syst. **4**, 559 (2017).

[36] Thomas G. Fai, Lishibanya Mohapatra, Prathitha Kar, Jane Kondev, and Ariel Amir, Length regulation of multiple flagella that self-assemble from a shared pool of components, eLife **8** (2019).

[37] Nils Gustafsson, Siân Culley, George Ashdown, Dylan M. Owen, Pedro Matos Pereira, and Ricardo Henriques, Fast live-cell conventional fluorophore nanoscopy with ImageJ through super-resolution radial fluctuations, Nat. Commun. **7**, 12471 (2016).

[38] William B. Ludington, Kimberly A. Wemmer, Karl F. Lechtreck, George B. Witman, and Wallace F. Marshall, Avalanche-like behavior in ciliary import, Proc. Natl. Acad. Sci. U.S.A. **110**, 3925 (2013).

[39] Nir Friedman, Long Cai, and X. Sunney Xie, Linking Stochastic Dynamics to Population Distribution: An Analytical Framework of Gene Expression, Phys. Rev. Lett. **97**, 168302 (2006).

[40] Madhura Bhave, Effrosyni Papanikou, Prasanna Iyer, Koushal Pandya, Bhawik Kumar Jain, Abira Ganguly, Chandrakala Sharma, Ketakee Pawar, Jotham Austin II, Kasey J. Day, Olivia W. Rossanese, Benjamin S. Glick, and Dibyendu Bhattacharyya, Golgi enlargement in Arf-depleted yeast cells is due to altered dynamics of cisternal maturation, J. Cell Sci. **127**, 250 (2014).

[41] Eugene Losev, Catherine A. Reinke, Jennifer Jellen, Daniel E. Strongin, Brooke J. Bevis, and Benjamin S. Glick, Golgi maturation visualized in living yeast, Nature (London) **441**, 1002 (2006).

[42] Kumi Matsuura-Tokita, Masaki Takeuchi, Akira Ichihara, Kenta Mikuriya, and Akihiko Nakano, Live imaging of yeast Golgi cisternal maturation, Nature (London) **441**, 1007 (2006).

[43] Inês G. Castro, David M. Richards, Jeremy Metz, Joseph L. Costello, Josiah B. Passmore, Tina A. Schrader, Ana Gouveia, Daniela Ribeiro, and Michael Schrader, A role for mitochondrial rho GTPase 1 (MIRO1) in motility and membrane dynamics of peroxisomes, Traffic **19**, 229 (2018).

[44] Sofie J. Huybrechts, Paul P. Van Veldhoven, Chantal Brees, Guy P. Mannaerts, Georgyi V. Los, and Marc Fransen,

Peroxisome dynamics in cultured mammalian cells, Traffic **10**, 1722 (2009).

[45] Christin Wallstab, Dimitra Eleftheriadou, Theresa Schulz, Georg Damm, Daniel Seehofer, Jürgen Borlak, Hermann-Georg Holzhütter, and Nikolaus Berndt, A unifying mathematical model of lipid droplet metabolism reveals key molecular players in the development of hepatic steatosis, FEBS J. **284**, 3245 (2017).

[46] Shengliu Wang, Yujia Zhai, Xiaoyun Pang, Tongxin Niu, Yue-He Ding, Meng-Qiu Dong, Victor W. Hsu, Zhe Sun, and Fei Sun, Structural characterization of coatomer in its cytosolic state, Protein Cell **7**, 586 (2016).

[47] Brock Roberts, Amanda Haupt, Andrew Tucker, Tanya Grancharova, Joy Arakaki, Margaret A. Fuqua, Angelique Nelson, Caroline Hookway, Susan A. Ludmann, Irina A. Mueller, Ruian Yang, Rick Horwitz, Susanne M. Rafelski, and Ruwanthi N. Gunawardane, Systematic gene tagging using CRISPR/Cas9 in human stem cells to illuminate cell organization, Mol. Biol. Cell **28**, 2854 (2017).

[48] D. S. Banerjee and S. Banerjee, Size regulation of multiple organelles competing for a shared subunit pool, PLoS Comput. Biol. **18**, e1010253 (2022).

[49] S. Patra and D. Chowdhury, Level crossing statistics in a biologically motivated model of a long dynamic protrusion: Passage times, random and extreme excursions, J. Stat. Mech. (2021) 083207.

[50] Srividya Iyer-Biswas, Gavin E. Crooks, Norbert F. Scherer, and Aaron R. Dinner, Universality in Stochastic Exponential Growth, Phys. Rev. Lett. **113**, 028101 (2014).